17th Australasian Fluid Mechanics Conference
Auckland, New Zealand
5-9 December 2010

Entrainment in turbulent fountain flow

N. Williamson[1], S. W. Armfield[1] and Wenxian Lin[2]

[1]School of Aerospace, Mechanical and Mechatronic Engineering, University of Sydney, NSW 2008, Australia

[2]School of Engineering & Physical Sciences, James Cook University, Queensland 4811, Australia

Abstract

Numerical simulations of turbulent fountain flow are used to investigate the important mass transfer mechanisms present in the forced fountain flow regime, which has been reported to exist at Froude numbers (Fr) greater than 3. The flow is equivalent to a negatively buoyant jet with three flow streams, the inner upflow (IF), the outer downflow (OF) and the surrounding ambient fluid (AF). Simulation results are presented for Fr = 4 and 7 at Reynolds number Re = 3350. The results suggest that the OF may be relatively well described by the dynamics of a pure line plume surrounding the IF but with higher entrainment owing to the unsteady pulsing behaviour of the flow entering the OF from the IF. The length scale for a pure plume appears to apply at Fr = 7 in the OF. Comparisons with previous results suggest the IF is not fully developed at Fr = 7 and entrainment into the IF from the OF may not occur until Fr > 15.

Introduction

In turbulent fountains or jets where a buoyancy force opposes the initial fluid motion, the flow rises to its maximum height and stagnates before forming an outer downflow (OF) which interacts with the inner flow (IF) and the ambient fluid (AF) as illustrated by the schematic in figure 1. Fountain flows occur widely in industrial and geophysical flows but are also an example of the more general shear mixing flow where the buoyancy force is aligned with the flow. Specific attention has been given to flow occurances in air–conditioning and heating in large buildings [2, 8], volcanic eruptions and the dynamics of cumulus cloud tops [12]. Fully turbulent fountain flow is characterised only by the Froude number,

$$\mathrm{Fr} = \left(\frac{M_0 W_0}{R_0 F_0}\right)^{1/2}, \qquad (1)$$

where R_0 is the radius of the source. M_0 and F_0 are the source momentum flux and the buoyancy flux defined as

$$M_0 = \int_0^{R_0} 2\pi r \overline{U_{z,0}}^2\, dr, \quad F_0 = \int_0^{R_0} 2\pi\sigma r \overline{U_{z,0}}\, dr,$$

where $\overline{U_{z,0}}$ is the time averaged vertical velocity at the source, σ is the reduced gravity between the fountain source and the ambient fluid and is defined as $\sigma = g(\rho_0 - \rho_\infty)/\rho_\infty$, with the subscript 0 indicating the fountain source and ∞ the ambient fluid. The characteristic velocity is $W_0 = Q_0/A_0$ with Q_0 and A_0 being the volume flow rate of the fountain at the source and source cross-sectional area respectively.

Kaye and Hunt [6] found that the fountain behaviour can be classified into three distinct regimes, 'very weak flow' for Fr < 1, 'weak flow' for 1 < Fr < 3 and 'forced flow' for Fr > 3. The identification of these regimes and the corresponding scaling relations for the fountain steady-state penetration depth Z_m, have been the subject of a number of studies [2, 12, 6, 10, 5, 14, 4, 13]. For Fr > 3 the flow approaches a linear scaling $Z_m/R_0 = C\,\mathrm{Fr}$, where C is a constant, or equivalently $Z_m \sim M_0^{3/4}/F_0^{1/2}$ as first identified by Turner [12] using dimensional arguments and laboratory experiments. Further experiments have shown this relation holds up to at least Fr ≈ 300 [2, 10]. Numerous other experiments support the scaling but there is some variation in the constant with, $C = 2.1 - 3.06$ [2, 12, 6, 5, 13].

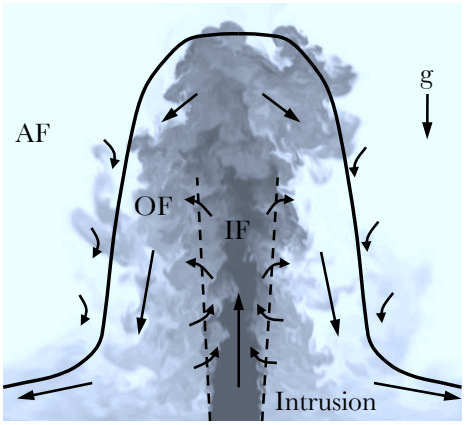

Figure 1: Turbulent fountain flow structure at Fr = 7 where shading indicates ϕ concentration.

Mizushina *et al.* [10] used anemometer probes to measure point velocity and temperature for fountain flow with Fr ≈ 5 – 260 and showed that unlike plumes or non-buoyant jets, in fountain flow, both the upflow and downflow continue to develop along their trajectories so the flow never attains self-similarity and the flow statistics vary with axial location and Froude number.

Using the integral model Morton [11] developed for plumes, Abraham [1] obtained analytically the linear high Froude number scaling. Kaye and Hunt [6] later obtained the same result with a similar approach and assuming entrainment in high Froude number forced fountains is similar to that in non-buoyant jets. In both studies only the initial upflow was considered, where the OF has not formed. Bloomfield and Kerr [4] extended the integral model of Morton [11] to fully established fountain flow by modifying the entrainment mechanism to include radial entrainment velocity ω from the IF into the OF (ω_β), the OF into the IF (ω_α) and the AF into the OF (ω_γ). The authors suggested two formulations for these entrainment processes. The most successful of these was the assumption that ω_α depends on the IF vertical velocity so $\omega_\alpha = \alpha W_{IF}$, where W_{IF} is the bulk IF vertical velocity. ω_β and ω_γ were assumed to depend on the OF vertical velocity only. The corresponding entrainment coefficients for these flow streams, α, β, γ were taken to be constant with height and Froude number. In testing the model they took $\alpha = 0.085$, based on earlier experiments on the initial rise of turbulent fountain flow in [3]. The coefficients γ and β were taken to be 0.147, a typical value for entrainment in a pure line plume. Results obtained by numerical integration of the equations compared well with the quantities available in Mizushina *et al.* [10], including the fountain width, velocity in

both streams and upflow buoyancy. The model was sensitive to the value of γ.

The apparent success of the Bloomfield and Kerr [4] approach suggests that the behaviour of the OF and the IF are essentially de-coupled and can be treated as two separate well understood flows, a plume and a jet. Understanding the mixing behaviour and the dynamics of the two streams (IF and OF) are critical for successful development of scaling models in more complex ambient environments. The measurements required to understand this behaviour are not currently available in the literature and most models are validated by comparing the fountain penetration height only. The objective of this work is to provide details of the flow behaviour in the forced flow regime and to give details of the mass exchanges between the IF, OF and AF. To this end direct numerical simulations have been obtained for turbulent fountain flow at $\mathrm{Fr} = 4$ and 7 and the results have been analysed.

Numerical formulation

We use direct numerical simulation (DNS) to solve the Navier–Stokes equations for incompressible flow and employ the Boussinesq approximation. The non-dimensionalised continuity, momentum and scalar transport equations are,

$$\frac{\partial u_i}{\partial x_i} = 0,$$

$$\frac{\partial u_i}{\partial t} + \frac{\partial (u_i u_j)}{\partial x_j} = -\frac{\partial p}{\partial x_i} + \frac{1}{\mathrm{Re}} \frac{\partial^2 u_i}{\partial x_j \partial x_j} - \frac{\phi}{\mathrm{Fr}_0^2},$$

$$\frac{\partial \phi}{\partial t} + \frac{\partial (u_j \phi)}{\partial x_j} = \frac{1}{\mathrm{Re}\,\mathrm{Pr}} \frac{\partial^2 \phi}{\partial x_j \partial x_j},$$

where Pr is the Prandtl number, the Reynolds number is defined as $\mathrm{Re} = W_0 R_0/\nu$ and ν is the kinematic viscosity of the fluid. The velocity (U_i), temperature (θ), pressure (P), time (T) and length (X_i) are made non-dimensional as $u_i = U_i/W_0$, $\phi = (\theta - \theta_\infty)/(\theta_0 - \theta_\infty)$, $p = P/\rho W_0^2$, $t = TW_0/R_0$ and $x_i = X_i/R_0$ respectively.

The discretised governing equations were solved in finite volume form on a non-staggered cartesian grid using a fractional step method. The spatial derivatives were discretised using second order central finite differences except for the scalar advective term which is nominally a second order centred scheme but with the ULTRA-flux limiter of [7] applied. The advective terms were advanced in time using the second order Adams–Bashforth scheme while the viscous terms were advanced using the Crank–Nicolson scheme. The equations were solved with the BICGSTAB solver with a Multi-grid Jacobi pre-conditioner. The computational domain is a rectangular box in which the top and side walls are open boundaries. The open boundaries have a zero gradient condition on the velocity and scalar field and zero second derivative on the pressure correction term. The bottom boundary is no-slip/adiabatic, except for the fountain source located in the centre where the normal velocity and temperature have uniform profiles at W_0 and ϕ_0.

We present results for the high Froude number flows $\mathrm{Fr} = 4$ and 7 at $\mathrm{Re} = U_0 R_0/\nu = 3350$ with $\mathrm{Pr} = 7$. The details of the simulation parameters are given in table 1. A regular Cartesian grid is used which is uniform in the horizontal x,y plane within a distance $Lu_{x,y}$ of the centre of the source. Outside this region the grid is stretched at approximately 5% growth-rate. The grid is uniform in the axial direction up to Lu_z and stretched at 3% thereafter. The source is prescribed as a uniform steady inlet profile.

Fr	Re	$\frac{\Delta X,Y}{R_0}, \frac{\Delta Z}{R_0}$	$\frac{L_{x,y}}{R_0}, \frac{L_z}{R_0}$	$N_{x,y}$,N_z	$\frac{Lu_{x,y}}{R_0}, \frac{Lu_z}{R_0}$
4.0	3350	0.03,0.06	16,17	293,197	3,9.5
7.0	3350	0.031,0.06	20,32	325,325	3.5,17

Table 1: Simulation parameters $\Delta X,Y,Z$, $L_{x,y,z}$ and $N_{x,y,z}$ give the grid size at the source, the domain size and the number of nodes respectively.

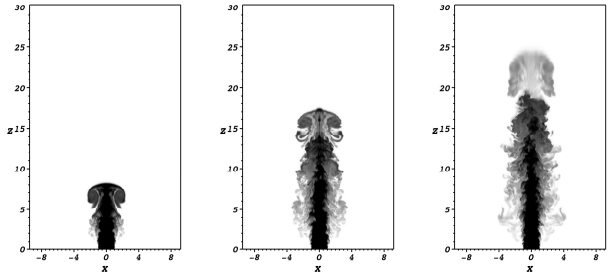

(*a*) (*b*) (*c*)

Figure 2: Startup flow at $\mathrm{Fr} = 7$ where shading indicates ϕ concentration and (*a-c*) are at $t = 16.7$, $t = 41.2$ and $t = 65.7$.

Results

After the simulations commence the fountains rise into the ambient domain and, at both $\mathrm{Fr} = 4$ and $\mathrm{Fr} = 7$, an annular vortex ring is formed at the head of the fountain. When the fountain reaches its maximum initial height this vortex ring separates from the fountain upflow and continues into the ambient domain mixing with ambient fluid as shown in figure 2. At $\mathrm{Fr} = 4$ gravity decelerates the vortex and it falls back to the source but at $\mathrm{Fr} = 7$ the vortex rises to the top of the simulated domain and escapes through the outlet. On reaching the maximum initial height the flow reverses and the OF is established followed by the intrusion along the bounding lower wall. The time trace of the source pressure and the maximum penetration height are given in figure 3. The maximum location at $r = 0$ where $\phi = 0.1$ gives the approximate location of the top of the detached vortex while the minimum location of $\phi = 0.1$ gives approximately the top of the fountain. For $\mathrm{Fr} = 7$, the vortex ring separates at $t \approx 65$. Most of the vortex leaves the top of the domain, with some of the fluid falling backwards to the source, meeting the fountain at $t \approx 200$. Flow statistics have been taken over $t \approx 200 - 310$. After start-up the source pressure is steady until $t \approx 80$ when it rises as the fountain outflow intrusion forms over the period $t \approx 80 - 150$, and is steady thereafter.

The fountain streams have been identified in figure 4 (a-b) for $\mathrm{Fr} = 4$ and $\mathrm{Fr} = 7$. The IF/OF boundary, r_{io} is defined as the radial location where the mean vertical velocity $\overline{u_z} = 0$. The best definition of the boundary between the OF/AF, r_{oa} is less clear. In an ideal pure plume ru_r is a constant and the plume width B is usually obtained from $\sqrt{(b^2W)^2/(b^2W^2)}$ where,

$$b^2 W = 2 \int_{r_1=0}^{r_2=\infty} \overline{u_z} r dr, \tag{2}$$

$$b^2 W^2 = 2 \int_{r_1=0}^{r_2=\infty} \overline{u_z}^2 r dr. \tag{3}$$

The equivalent length scale for a fountain OF half-width is,

$$B_{1/2} = \left(\left(2 \int_{r_d}^{r_{\mathrm{lim}}} \overline{u_z} r dr \right)^2 \Big/ \left(2 \int_{r_d}^{r_{\mathrm{lim}}} \overline{u_z}^2 r dr \right) + r_d^2 \right)^{1/2} - r_d. \tag{4}$$

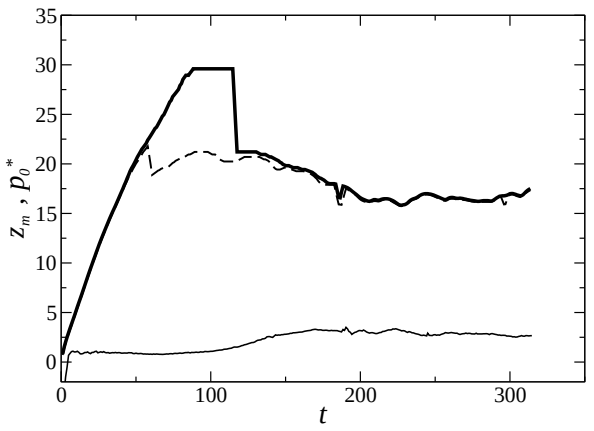

Figure 3: Time evolution of fountain height at $r = 0$ and normalised source pressure head $p_0^* = p_0 \mathrm{Fr}^2$, at $r = 0$ and $z = 0$ for $\mathrm{Fr} = 7$. $p_0^*(t)$ is indicated by thin-solid lines. The thick solid line indicates the maximum location of $\phi = 0.1$, which gives the approximate location of the top of the detached vortex. The dashed-line indicates minimum location of $\phi = 0.1$ which gives the approximate location of the fountain height $z_m(t)$.

The simulated domain is finite so the integrals in (4) are evaluated to the edge of the domain $r = r_{\mathrm{lim}}$. The total distance from the centreline is $r_{oa} = B_{1/2} + r_d$. This definition of r_{oa} is plotted in figure 4. A second definition defined as the location where $\phi = 0.025$ is also given in figure 4. The value $\phi = 0.025$, is arbitrary and it will be shown later that the entrainment calculations are not sensitive to its value. The comparison between this definition and that based on (4) shows that they are only close over a small portion of the OF height with large deviations at the top and bottom of the flow height. The ambient fluid is not quiescent above z_m but has a velocity profile that extends into the domain a long distance above the location $\overline{\phi} \approx 0$, which has the affect of increasing the length-scale in (4). Additionally the intrusion affects the flow below $z = 4$ at $\mathrm{Fr} = 7$ so the length scale is not expected to apply in this region. The downward flow of the OF and the outward motion of the intrusion along the wall produces a weak circulation cell in the AF. This circulation may also have a small affect on the result.

The inner upflow stream expands rapidly over $z = 0 - 2$ for $\mathrm{Fr} = 4$ and $z = 0 - 4$ for $\mathrm{Fr} = 7$ and then expands very slowly at approximately $dr/dz \approx 0.04$ as shown in figure 4. The maximum velocity in the OF is located at $r \approx 2.5$ and $r \approx 3.0$, largely independent of z, for $\mathrm{Fr} = 4$ and $\mathrm{Fr} = 7$ respectively. The IF contracts after $z \approx 7$ and $z \approx 11.5$ for $\mathrm{Fr} = 4$ and $\mathrm{Fr} = 7$ respectively. The downflow expands at the base of the fountain as the plume moves into the intrusion.

It is attractive from a modelling point of view to treat the OF as an independent plume, a flow which is relatively well understood. The integral length scale L_{11} for radial variance $\overline{u_r'(r,z)u_r'(r+dr,z)}$ is given as,

$$L_{11}(r,z) = \int_r^{r_{\mathrm{lim}}} \frac{\overline{u_r'(r,z)u_r'(r+dr,z)}}{\sqrt{\overline{u_r'(r,z)}^2}\sqrt{\overline{u_r'(r+dr,z)}^2}}\, dr.$$

This result is plotted in figure 5 for $\mathrm{Fr} = 7$. The length scale is relatively flat across the IF region but rises sharply over $r = r_{io} - r_d$. In the OF region over $r = 2.5 - 6$, the length scale increases to $L_{11} = 2$ for $\mathrm{Fr} = 7$, which is approximately half the width of the OF stream. These relatively small length scales

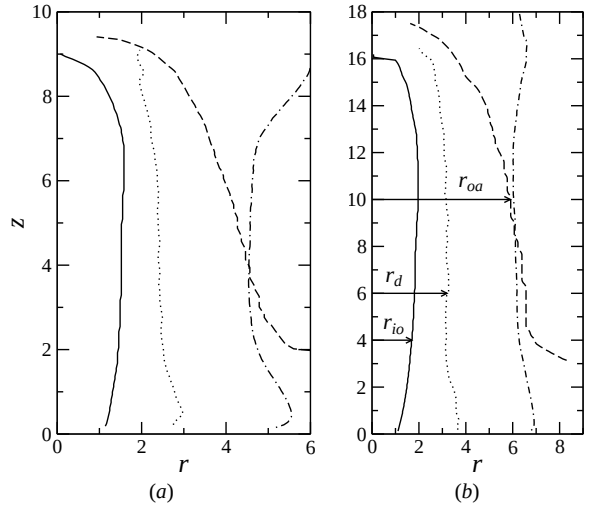

Figure 4: Boundaries between flow streams in $\mathrm{Fr} = 4$ (a) and $\mathrm{Fr} = 7$ (b). Solid line - IF/OF boundary where $\overline{u_z} = 0$; dotted line - $r_d(z)$; dashed line - OF/AF boundary where $\overline{\phi} = 0.025$; dashed–dotted line - $B_{1/2} + r_d$.

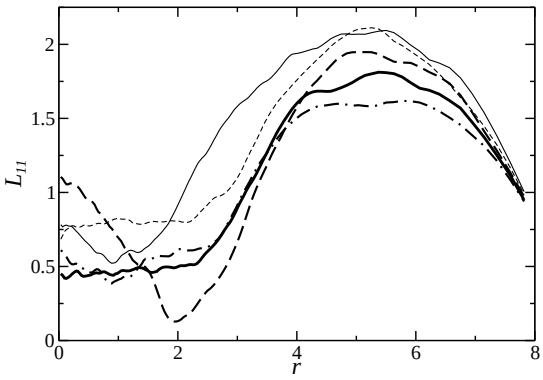

Figure 5: L_{11} for $\mathrm{Fr} = 7$. The lines dash–dotted, thick solid, thick dashed, thin dashed, thin solid indicate $z = 4$, $z = 6$, $z = 8$, $z = 10$, $z = 12$.

suggest the connection between the structures in the IF and the OF is fairly indirect and allows the possibility that the OF may be treated separately.

The mean entrainment α between the streams is calculated as

$$\alpha = -s\overline{u_r}/W, \tag{5}$$

where $\overline{u_r}$ is obtained at r_{io} for IF/OF entrainment and at r_{oa} for OF/AF entrainment. The entrainment direction is into the OF from both the AF and the IF over most of the height. This direction is taken as positive so $s = -1$ for the AF/OF boundary and $s = 1$ for the IF/OF boundary. The bulk OF stream velocity is given as,

$$W = \frac{b^2W^2}{b^2W},$$

where b^2W^2 and b^2W are defined in (2) and (3) and $r_1 = 0$ and $r_2 = r_{io}$ for the IF stream and $r_1 = r_{io}$ and $r_2 = r_{oa}$ for the OF stream.

The entrainment rate is plotted in figure 6 for $\mathrm{Fr} = 4$ and $\mathrm{Fr} = 7$. Results for multiple definitions of r_{oa} are presented and the

sensitivity of the entrainment rate to boundary location is also given. The entrainment profile from the AF with $r_{oa} = r_{\rm lim}$ is also shown in figure 6. The entrainment rate is not sensitive to the location of the boundary.

The entrainment profiles illustrate three distinct regions of behaviour. In region 1, over $z = 0-2$ for Fr $= 4$ and $z = 0-4$ for Fr $= 7$, there is entrainment into the IF from the OF and from the OF into the base intrusion or AF. In region 2, for $z \approx 2-8$ for Fr $= 4$ and $z \approx 4-14$ for Fr $= 7$, there is entrainment from the AF to the OF with $\overline{\alpha} = 0.1-0.2$. Over this region there is low entrainment into the OF from the IF. In region 3, for $z \approx 8-z_m$ for Fr $= 4$ and $z \approx 14-z_m$ for Fr $= 7$ the entrainment regime in both streams is dominated by ejection of fluid from the cap region, so the OF receives fluid from the IF and the AF receives fluid from the OF.

In regions 1 and 3 the flow behaviour shown in figure 6 is unlikely to depend on W and so is not an entrainment mechanism in the same sense as that observed in a plume or jet. In region 2 however the behavior may be reasonably well compared to these ubiquitous flows. List [9] gives the entrainment into a plane buoyant plume as $\alpha = 0.14$ while entrainment into an axisymetric plume has $\alpha = 0.11$. The slightly higher entrainment coefficient found here between the AF and OF may be due to the ambient circulation or the more unsteady pulsing behaviour of the ejection into the OF. The dense fluid enters the OF with higher radial velocity and therefore once it accelerates down it is able to draw more ambient fluid in behind each pulse than would otherwise occur in a less unsteady flow.

The very low mean entrainment from the IF to the OF in region 2 indicates that most of the mass exchange occurs via $\overline{u_r' u_z'}$ and $\overline{u_r' \phi'}$. Mizushina *et al.* [10] gives the expansion rate of the IF for higher Froude number flow over Fr $= 15-70$ at $\Delta r_{io}/\Delta z = 0.15-0.23$. With a top hat velocity profile this result indicates $\alpha \approx 0.075-0.115$, with α appearing to decrease with increasing Froude number. These values lie between the typical value for a jet $\alpha = 0.075$ and that for a plume $\alpha = 0.11$. This result then supports the hypothesis that the IF behaves like a jet at very high Froude number and that our result is in a regime where the IF is not fully developed.

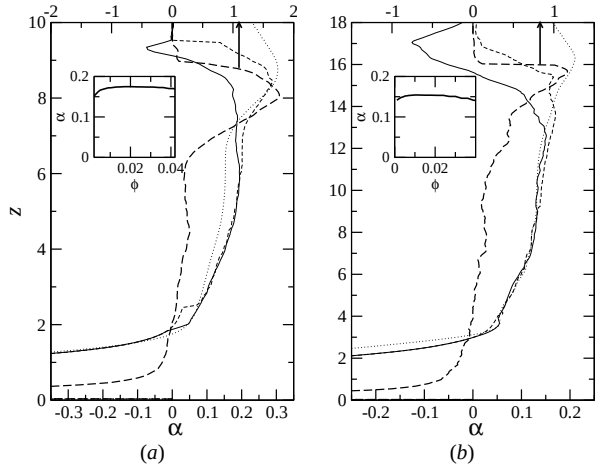

Figure 6: Mean entrainment rates for Fr $= 4$ (*a*) and Fr $= 7$ (*b*). Entrainment into OF from IF - thick dashed line; entrainment into OF from the AF with the OF/AF boundary r_{oa} defined by the location of $\phi = 0.025$ - Solid line, $\phi = 0.005$ - thin dashed line and $r_{\rm lim}$ - dotted line. Inner plot indicates sensitivity of AF entrainment to r_{oa}, as defined by ϕ, at $z = 5$ and $z = 11$ for Fr $= 4$ (*a*) and Fr $= 7$ (*b*) respectively.

Conclusions

Numerical simulations of turbulent fountain flow have been used to investigate the behavior of turbulent fountain flow at Fr $= 4$ and 7 at Reynolds number Re $= 3350$. The results suggest that the mean entrainment of ambient fluid into the outer downflow is higher than in an axisymmetric or plane plume. It is hypothesised that this is due to the unsteady pulsing behaviour of the flow entering the OF from the IF. The relevant length scale in the outer downflow is relatively well approximated by the length scale for a pure plume for Fr > 7. Comparisons with previous results suggest the IF is not fully developed at Fr $= 7$ and entrainment into the IF from the OF may not occur until Fr > 15.

References

[1] Abraham, G., Jets with negative buoyancy in homogeneous fluid, *J. Hyd. Res.*, **5**, 1967, 235–248.

[2] Baines, W. D., Turner, J. S. and Campbell, I. H., Turbulent fountains in an open chamber, *J. Fluid Mech.*, **212**, 1990, 557–592.

[3] Bloomfield, L. J. and Kerr, R. C., Turbulent fountains in a stratified fluid, *J. Fluid Mech.*, **358**, 1998, 335–356.

[4] Bloomfield, L. J. and Kerr, R. C., A theoretical model of a turbulent fountain, *J. Fluid Mech.*, **424**, 2000, 197–216.

[5] Campbell, I. H. and Turner, J. S., Fountains in magma chambers, *J. Petrol.*, **30**, 1989, 885–923.

[6] Kaye, N. B. and Hunt, G. R., Weak fountains, *J. Fluid Mech.*, **558**, 2006, 319–328.

[7] Leonard, B. P. and Mokhtari, S., Beyond first-order upwinding: the ultra-sharp alternative for non-oscillatory steady state simulation of convection, *Int. J. Numer. Meth. Engng*, **30**, 1990, 729–766.

[8] Lin, Y. J. P. and Linden, P. F., The entrainment due to a turbulent fountain at a density interface, *J. Fluid Mech.*, **542**, 2005, 25–52.

[9] List, E. J., Turbulent jets and plumes, *Ann. Rev. Fluid Mech.*, **14**, 1982, 189–212.

[10] Mizushina, T., Ogino, F., Takeuchi, H. and Ikawa, H., An experimental study of vertical turbulent jet with negative buoyancy, *Wärme-und Stoffübertragung*, **16**, 1982, 15–21.

[11] Morton, B. R., Forced plumes, *J. Fluid Mech.*, **5**, 1959, 151–163.

[12] Turner, J. S., Jets and plumes with negative or reversing buoyancy, *J. Fluid Mech.*, **26**, 1966, 779–792.

[13] Williamson, N., Srinarayana, N., Armfield, S. W., McBain, G. D. and Lin, W., Low-reynolds-number fountain behaviour, *J. Fluid Mech.*, **608**, 2008, 297–317.

[14] Zhang, H. and Baddour, R. E., Maximum penetration of vertical round dense jets at small and large Froude numbers, *J. Hydraulic Eng.*, **124**, 1998, 550–553.